JOURNAL OF GEOPHYSICAL RESEARCH, VOL. 91, NO. B7, PAGES 7485–7494, JUNE 10, 1986

Phase Transitions, Grüneisen Parameter, and Elasticity for Shocked Iron Between 77 GPa and 400 GPa

J. MICHAEL BROWN[1]

Geophysics Program, University of Washington, Seattle

ROBERT G. MCQUEEN

Shock-Wave Physics Group, Los Alamos National Laboratory, Los Alamos, New Mexico

Sound velocities determined in iron, shock compressed to pressures between 77 GPa and 400 GPa, indicate that two phase transitions exist on the Hugoniot. A discontinuity in sound velocities at 200 ± 2 GPa may mark the transition of ε iron to γ iron. A second discontinuity at 243 ± 2 GPa is believed to indicate the onset of melting. The calculated temperature at melting lies between 5000 K and 5700 K. When extrapolated from the Hugoniot melting point, the Lindemann criterion yields an estimate of 5800 ± 500 K for the melting of pure iron at the inner core boundary pressure of 330 GPa. The product of density times the thermodynamic Grüneisen parameter in liquid iron, calculated from the present data, is 19.6 ± 0.8 Mg m^{-3}. A temperature profile ranging from 3800 K at the core-mantle boundary to 5000 K at the earth's center is calculated using the present data. Sound velocities for ε iron provide a better match to seismic velocities for the earth's inner core than do those of γ iron. A comparison between liquid iron velocities and the velocity profile through the outer core provides further evidence for alloying of iron with "lighter elements" in the core.

INTRODUCTION

We previously described a new high-pressure shock wave technique that makes it possible to determine the sound velocity in shocked material [*Brown and McQueen*, 1980]. If the material is in the solid state, the velocity of longitudinal elastic waves is measured. For a liquid, the bulk sound velocity (K/ρ where, K is the isentropic bulk modules and ρ is density) is determined. These experiments provide information not previously resolvable in shock wave data. Prior to a description of the new method, we describe the conventional shock wave technique. Typically, Hugoniot states are characterized using measurements of shock velocity (U_s) and particle velocity (U_p). Through the Rankine-Hugoniot relations, these data define a compression curve (density versus pressure) as a function of known Hugoniot energy. Although this method provides valuable equation-of-state information, it is difficult or impossible to determine where melting or where phase transitions with small volume changes occur [e.g., *McQueen et al.*, 1970]. Furthermore, reduction of shock data to isothermal or isentropic states requires specific heat and Grüneisen parameter (γ) values that are not well known. In the absence of experimental constraints, plausible speculation has been necessary (see, for example, *Jamieson et al.* [1978], *Ahrens* [1979], and *Brown et al.* [1984]).

In contrast to standard Hugoniot data, the current experimental method involves determination of the velocity of a pressure release wave that propagates behind and overtakes the shock front. The determination of the bulk sound velocity in a liquid provides a direct measure of the isentropic modulus: $\partial P/\partial V_s$, where P is pressure and V is volume. In combination with standard Hugoniot results, such new data provide a direct measure of the thermodynamic Grüneisen parameter. Furthermore, a phase transition causing only a minor kink in compression data can produce a marked discontinuity in elastic sound velocities. The present technique thus provides a powerful tool to explore high-pressure phenomena [*Brown and Shaner*, 1984; *Brown et al.*, 1985; *Swenson et al.*, 1986].

Experimental constraints on the behavior of the Grüneisen parameter for iron under deep earth condition have been limited and are not in complete agreement. *Ramakrishnan et al.* [1978] measured γ for α iron (body-centered cubic) to 3.3 GPa at room temperature. Using the parameterization

$$\gamma = \gamma_0\left(\frac{\rho_0}{\rho}\right)^n \tag{1}$$

where subscript 0 implies values under ambient conditions, they found $n = 0.6$. *McQueen et al.* [1970] provided Grüneisen parameter estimates to more than 100 GPa based on finite differences in thermal pressure between porous and nonporous Hugoniot data. However, interpretation of these results is complicated by extreme differences in thermodynamic state between the porous and nonporous data. McQueen et al. found $n = 1$ to be a reasonable approximation to their somewhat scattered data. *Jeanloz* [1979] reconsidered the same porous Hugoniot data and proposed that n is equal to 1.62. At high compression this latter parameterization differs little from the *McQueen et al.* [1970] interpretation.

Preliminary sound velocity data for iron have been given in a graphical presentation [*Brown and McQueen*, 1980] where the existence of two phase transitions above 100 GPa were indicated. An additional analysis [*Brown and McQueen*, 1982] provided further evidence that the transition at 200 GPa represents the ε (hexagonal close packed) to γ (face-centered cubic) transition, while the higher-pressure discontinuity is caused by melting of γ iron. We note that sound velocities for iron in the 100-GPa pressure regime were reported by *Al'tshuler et al.* [1960, 1971]. However, there were inconsistencies between these two papers and with current results. Fur-

[1] Formerly at Geophysics Department, Texas A&M University, College Station.

Paper number 6B5970.
0148-0227/86/006B-5970$05.00

thermore, using the Russian technique, many separate experiments were required to make one velocity determination. We emphasize that the current technique has significantly better resolution, and the earlier Russian data are not considered further.

We have now obtained additional data for iron extending the pressure regime from 77 GPa to 400 GPa. In combination with data in the range of 10 to 40 GPa [*Barker and Hollenbach*, 1974], sound velocities in shocked iron are constrained over an extensive pressure regime through three phase transitions. The lowest-pressure transition from α iron to ε iron at approximately 13 GPa has been thoroughly studied using both shock wave [*Johnson et al.*, 1962; *Barker and Hollenbach*, 1974] and static [*Jamieson and Lawson*, 1962; *Mao et al.*, 1967; *Jephcoat et al.*, 1986] techniques. From 40 Gpa to 200 GPa, sound velocities increase smoothly and appear to represent longitudinal elastic waves in ε iron. Between 200 GPa and 243 GPa, we infer that velocities represent longitudinal sound waves in γ iron. Above 243 GPa, velocities are consistent with properties of liquid iron. Values for the bulk sound velocity of liquid iron allow the thermodynamic parameter $\partial E/\partial P_v$ ($= (\rho\gamma)^{-1}$) to be determined. A constant value of 0.051 ± 0.002 m^3 Mg^{-1} is suggested by the data. This value lies within bounds provided by porous iron results, where data were scattered between 0.04 m^3 Mg^{-1} and 0.08 m^3 Mg^{-1} [*McQueen et al.*, 1970]. In contrast, the low-pressure static data of *Ramakrishnan et al.* [1978] gave a value of 0.077 m^3 Mg^{-1} for α iron at room temperature. Using velocity-density systematics, we also conclude that the inner core has thermodynamic (equation-of-state) properties not unlike pure ε iron. A core geotherm is proposed with temperatures ranging from 3800 K at the core-mantle boundary to 5000 K at the earth's center.

SHOCK WAVE "EQUILIBRIUM"

We make the assumption that present experimental results represent "equilibrium" behavior despite the "short" time scale of measurement. Furthermore, we assert that the shock process can generate a nearly hydrostatic high-pressure state with finite rigidity. These problems of equilibrium and rheology in shock waves are of continuing concern and have been extensively considered, both experimentally and theoretically. Although unambiguous conclusions may be premature, we believe that near-equilibrium, hydrostatic states are obtained; these points were previously discussed by *Davison and Graham* [1979]. We provide a brief review incorporating more recent work.

Discussions of thermodynamic equilibrium in shocked materials must be organized into separate questions of thermalization and metastability. Thermalization is achieved when a system has a Maxwell distribution of occupied phonon states. This is necessary in order to define temperature as a state variable. A thermalized material may, for kinetic reasons, remain in a metastable state, rather than relax to a lower free-energy equilibrium phase. This potential problem of metastability is not unique to shock experiments and is further discussed below.

Holian and Straub [1979] addressed the problem of thermalization using molecular dynamics calculations. They recognized the critical problem that longitudinal energy imparted by the shock process must be partitioned into transverse modes. Under ambient conditions, phonon-phonon scattering results in slow thermalization. However, equilibration is reduced to a picosecond time scale in a strong shock. An enhanced scattering cross section results from very anharmonic lattice distortions near the shock front.

Molecular dynamics calculations also support the validity of the Rankine-Hugoniot equations. The shock front is calculated to be as thin as a few tens of lattice spacings. Despite the intense deformation and "bond breaking" processes at the shock front, material is calculated to reorganize into an ordered structure. Thus rigidity can be expected in the shocked material. Holian and Straub further recognize a threshold between "weak" and "strong" shock behavior. For low-pressure shock waves, thermalization processes are less effective. The result is a broad shock front, incomplete thermalization, and a nonhydrostatic stress distribution in the shocked material. This low-pressure regime roughly corresponds to a range near the "Hugoniot elastic limit" which is typically less than 10 GPa for metals.

On the basis of existing experimental data, the degree of "hydrostaticity" in shocked samples is still uncertain. However, *Morris and Fritz* [1980] placed upper bounds on deviatoric stresses in aluminum and copper shocked to the 100-GPa regime. They found maximum values of the order of a few percent of the Hugoniot pressure. Although nonhydrostatic stresses are likely to be nonzero in the present data, we conclude that the effects of such nonhydrostaticity on our interpretations are negligible.

Empirical evidence can be given in support of equilibrium behavior through phase transitions in at least some shocked materials. The low-pressure phase boundaries for α, γ, and ε iron were initially determined using shock waves [*Johnson et al.*, 1962]. This phase diagram is in agreement with later static work. The room temperature isotherm for ε iron, reduced from shock data, is in excellenet agreement with the recent static data of *Jephcoat et al.* [1986]. The quartz to stishovite transition initiates at approximately the same pressure in static [*Akimoto and Syono*, 1969] and dynamic experiments [*Wackerle*, 1962]. Furthermore, pulse X ray diffraction studies have demonstrated both that a transition to a high-pressure ordered phase can occur in a shock experiment and that the structure is identical to what is observed in static studies [*Johnson and Mitchell*, 1972].

A number of shocked materials do appear to remain in a low-pressure phase beyond equilibrium phase boundaries. Examples include the graphite $\rightarrow$ diamond and olivine $\rightarrow$ post-olivine transitions [*Marsh*, 1980]. In these cases, however, Hugoniot temperatures are low at the equilibrium phase boundary (of the order of 300–500 K), and these transitions are quite sluggish in static experiments under similar thermal conditions of temperature and pressure. Approximate temperatures for the initiation of Hugoniot phase transitions in these materials are estimated to be of the order of 1000 K. This agrees with typical conditions necessary to achieve synthesis of high-pressure phases under static conditions (see, for example, *Bundy* [1980] and *Furnish and Bassett* [1983]).

The question of whether equilibrium melting can be observed in the short time scale of shock measurements has been experimentally answered by *Asay* [1977] and *Asay and Hayes* [1975]. They studied bismuth and porous aluminum. These materials melt at temperatures low enough for direct comparisons between shock and static data. They noted that when the Hugoniot crossed the solidus, the velocity of the release sound wave dropped rapidly from the longitudinal to the bulk sound velocity. These velocities differed by approximately 30%.

The preceding work is suggestive but certainly not con-

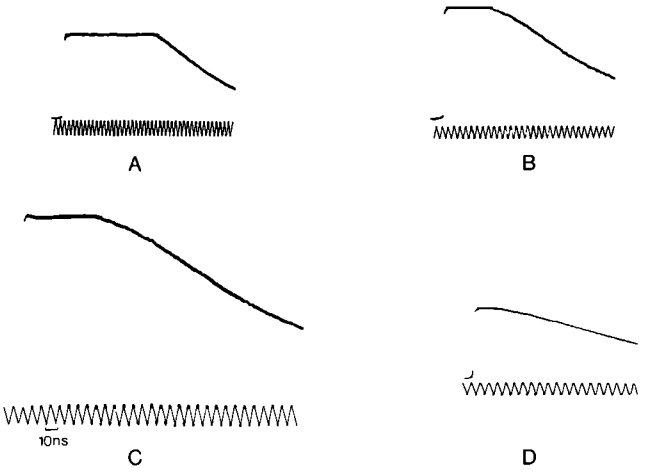

Fig. 1. Photomultiplier records for an overtaking rarefaction sound velocity experiment. Target thickness increases from Figures 4*a* to 4*d*.

clusive. Nonhomogenous behavior has been observed in some low-pressure shock wave experiments [*Kondo and Ahrens*, 1983; *Grady and Asay*, 1982]. However, for a monoatomic, close-packed material like iron, with a relatively low yield strength (~2 GPa), it appears that existing research supports our assumptions of equilibrium for shock wave experiments in the 100-GPa pressure regime.

Overtaking Rarefaction Method

The experimental technique has been described elsewhere [*Brown and McQueen*, 1980; *McQueen et al.*, 1982]. However, a discussion is included here for completeness and to allow assessment of experimental uncertainties.

The impact of a thin plate on a target causes a shock wave to propagate into both. When the shock wave reaches the back surface of the impactor, pressure is released and a rarefaction sound wave propagates forward through the system. This wave travels through the impactor, into the target, and eventually overtakes the shock front in the target. The thickness of the target at the overtaking point is determined (as described later), and R is defined as the ratio of that thickness to the impactor thickness. For symmetric impacts (i.e., flyer and target are the same material), the quantity R^* is defined:

$$R^* = (R + 1)/(R - 1) \tag{2}$$

which is related to the Eulerian sound velocity, C, by

$$R^* = \left(\frac{\rho}{\rho_0}\right)\frac{C}{U_s} \tag{3}$$

For a solid, C represents the longitudinal (compressional) elastic velocity, V_p, whereas for a liquid with no shear strength, C represents the bulk sound velocity, V_B. The two velocities are related through Poisson's ratio, σ, by

$$\left(\frac{V_p}{V_B}\right)^2 = 3\frac{(1-\sigma)}{(1+\sigma)} \tag{4}$$

In order to extend the experimentally accessible pressure range, nonsymmetric impacts are required, using a higher shock impedance impactor. In this case, subscripts T and D refer to properties of the target and driver (also called the flyer), respectively. The experimentally observed ratio, R_{exp}, depends on properties of both driver and target:

$$R_{exp} = \frac{U_{sT}}{U_{sD}}(R_T + 1)\left(\frac{R_D}{R_D + 1}\right) \tag{5}$$

We have, in separate symmetric impact experiments, measured R_D for tantalum as a function of Hugoniot pressure [*Brown and Shaner*, 1984]. Thus for a given state generated in an impact of tantalum on iron, we have sufficient data to solve equation (5) for R_T, which can be used in (2) and (3) to calculate the sound velocity.

The bulk sound velocity is used to calculate the thermodynamic quantity $\partial E/\partial P_v$ from the following equation:

$$\frac{\partial E}{\partial P_v} = \frac{[(\partial E/\partial V_H) - (\partial E/\partial V_S)]}{[(\partial P/\partial V_H) - (\partial P/\partial V_S)]} \tag{6}$$

Here $\partial E/\partial P_v$ is represented as the ratio of the difference between slopes on the Hugoniot (subscript H) and on the isentrope (subscript S) and E is internal energy. Using the Rankine-Hugoniot relations, a linear shock particle velocity Hugoniot ($U_s = C_0 + sU_p$), and the thermodynamic law, $dE = TdS - PdV$, equation (6) can be rewritten:

$$\frac{\partial E}{\partial P_v} = \frac{1}{\rho\gamma} = \frac{s\eta^2}{\rho_0}[(1 + s\eta) - R^{*2}(1 - s\eta)]^{-1} \tag{7}$$

where $\eta = U_p/U_s = (V_0 - V)/V_0$.

An optical analyzer technique was used to determine the target thickness at the rarefaction overtaking point. A transparent material (either bromoform or leaded glass) was placed in contact with steps of different thickness on the target. Shock propagation through the analyzer generates large shock heating, accompanied by copious thermal radiation in the visible spectrum. If the material radiates like a black body, then, by Planck's Law, the total radiation intensity is proportional to the fourth power of temperature. Temperature, in turn, increases rapidly with pressure on the Hugoniot. Hence small changes in pressure result in large changes in radiation. The overtaking of the shock front by the rarefaction sound wave in the analyzer causes a reduction in pressure and temperature, which results in a sharp decrease in thermal radiation. The

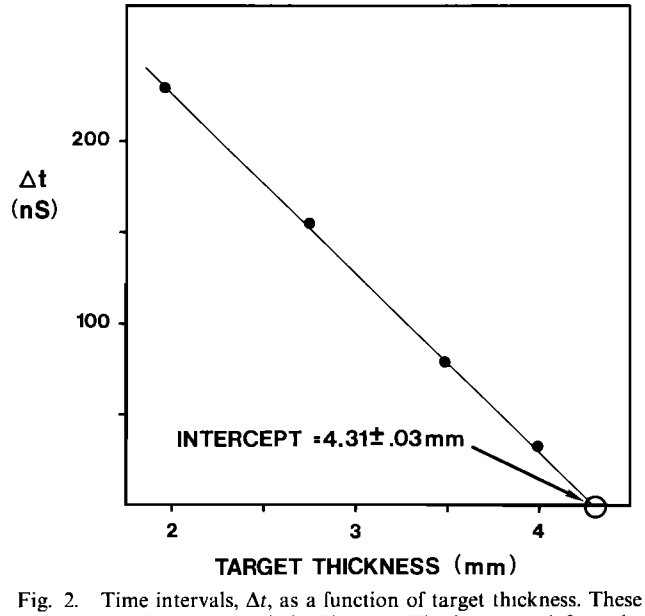

Fig. 2. Time intervals, Δt, as a function of target thickness. These were measured for the records in Figure 1. The intercept defines the thickness of the target at the point where the rarefaction wave overtakes the shock front.

TABLE 1. Sound Velocity Data for Iron: Explosive Experiments

Experiment	U_s, km/s	U_p, km/s	Pressure, GPa	Density, Mg/m^3	R	Sound Velocity, km/s	$\partial E/\partial P_v$, m^3/Mg
8C3619	7.25 (3)	2.09	119 (2)	11.02 (7)	3.73 (2)	8.95 (3)	···
8C3620	7.27 (3)	2.10	120 (2)	11.04 (7)	3.73 (2)	8.96 (3)	···
8C3635	7.67 (3)	2.35	142 (2)	11.32 (7)	3.86 (4)	9.04 (12)	···
8C3637	8.26 (2)	2.73	177 (2)	11.71 (7)	3.87 (10)	9.39 (13)	···
8C3639	8.68 (6)	2.99	204 (3)	11.98 (8)	3.73 (6)	9.86 (7)	···
8C3648	8.73 (6)	3.02	207 (3)	12.01 (8)	4.01 (6)	9.50 (7)	···
8C3645	8.92 (3)	3.14	220 (2)	12.12 (7)	4.09 (6)	9.52 (7)	···
8C3646	9.25 (2)	3.35	243 (2)	12.31 (7)	4.04 (5)	9.78 (6)	···
8C3638	9.67 (12)	3.62	275 (8)	12.54 (11)	4.39 (6)	9.62 (7)	0.051 (4)

Values in parentheses are uncertainties in least significant figures.

variation in target thicknesses leads to different time intervals between emergence of the shock in the analyzer and overtaking of the shock by the sound wave.

We detect visible light from the optical analyzer above each target level. Apertures and baffles collimate light onto silica optical fibers, which transmit the light to fast (1-ns rise time) and linear photomultiplier detectors [*Beck*, 1976]. Single-sweep, internally triggered oscilloscope records are obtained for all target thicknesses.

Photographic records for one experiment are reproduced in Figure 1. A discontinuous increase in signal amplitude occurs as the shock emerges from the iron into the analyzer. Nearly constant thermal radiation is observed as the shock moves through the analyzer. The rarefaction overtaking point is indicated by a decrease in radiation. Details of the pressure-releasing part of these records is complicated by iron-analyzer interactions as well as nonideal "elastic-plastic" deformation in the iron. However, we emphasize that, independent of these complications, the velocity of the fastest release wave can clearly be determined.

The time interval, Δt, between emergence of the shock and the overtaking point is measured with a reproducibility of a few nanoseconds. These values are plotted against target thickness (Figure 2). A short linear extrapolation defines the point at which the rarefaction would overtake the shock front in the target.

The standard deviation of linear regression parameters provides an estimate of uncertainties. On this basis, the precision in determination of R can approach 0.5%. Accuracy may be affected by finite time responses, causing a potential bias in the choice of arrival times. Observed rise times for shock-induced radiation range from 2 ns to over 10 ns. The smaller value is at the limit imposed by optical dispersion in the fiber cables and the response of the electronic system. Longer rise times may represent several phenomena including (1) tilt or other nonplanar distortions of the shock front over the area viewed or (2) a finite thickness of the shock front. Even in worst case situations, different criteria for the choice of arrival times shift overtake ratios by no more than a few percent. Since the overtake ratios, R, are typically about 4, it can be seen from equations (2) and (3) that the sound velocities have an accuracy of approximately 1%. Errors in the determination of shock pressure are relatively unimportant, since the overtake ratio is a slowly varying function of shock pressure. A slightly incorrect shock velocity determination moves a release velocity primarily along the trend of the data. However, pressures must be well determined near phase transitions if transition pressures are to be well constrained.

EXPERIMENTAL RESULTS

Both explosive-driven and two-stage light-gas gun shock wave experiments have been conducted on iron. The material studied was low-carbon, cold-rolled steel (C1015) with a purity of approximately 99%. This material is a standard for shock wave research. Major impurities include carbon (<0.2%), manganese (<0.7%), and silicon (<0.1%). Physical properties

TABLE 2. Sound Velocity Data for Iron: Two-Stage Light-Gas Gun Experiments

Experiment	Impactor	Impact Velocity, km/s	U_s, km/s	Pressure, GPa	Density, Mg/m^3	R	Sound Velocity, km/s	$\partial E/\partial P_v$, m^3/Mg
397*	Fe	3.061 (3)	6.37 (4)	77 (1)	10.33 (4)	3.95 (3)	8.13 (4)	···
396*	Fe	3.742 (4)	6.91 (4)	102 (1)	10.76 (4)	3.87 (3)	8.55 (4)	···
334*	Fe	4.914 (5)	7.82 (4)	151 (1)	11.44 (4)	3.74 (3)	9.31 (5)	···
276	Fe	5.764 (6)	8.51 (4)	193 (1)	11.87 (4)	3.78 (6)	9.67 (7)	···
272	Fe	5.824 (6)	8.56 (4)	196 (1)	11.90 (4)	3.74 (5)	9.76 (7)	···
275	Fe	5.930 (6)	8.64 (4)	201 (1)	11.95 (4)	3.91 (4)	9.57 (5)	···
273	Fe	6.024 (6)	8.71 (4)	206 (1)	12.00 (4)	4.10 (2)	9.38 (3)	···
274	Fe	6.511 (7)	9.10 (5)	233 (1)	12.22 (4)	4.07 (4)	9.65 (5)	···
329*	Fe	6.728 (7)	9.27 (5)	245 (1)	12.32 (4)	4.10 (2)	9.72 (3)	···
330*	Fe	6.838 (7)	9.36 (5)	251 (1)	12.37 (4)	4.17 (2)	9.68 (5)	···
277	Fe	6.994 (7)	9.48 (5)	260 (1)	12.44 (4)	4.34 (4)	9.57 (5)	0.053 (2)
296	Ta	6.929 (7)	10.40 (6)	333 (2)	12.92 (4)	4.27 (3)	10.19 (4)	0.049 (2)
340*	Ta	7.768 (7)	11.17 (6)	400 (2)	13.28 (4)	4.06 (3)	10.91 (4)	0.050 (2)

Values in parentheses are uncertainties in least significant figures.
*Data not previously shown in the work of *Brown and McQueen* [1980, 1982].

TABLE 3. Calculated Properties for Iron on the Hugoniot

Pressure, GPa	Temperature, K	Density, Mg/m^3	Bulk Sound Velocity, km/s
40	655	9.49	5.67
60	969	9.99	6.21
80	1,355	10.40	6.67
100	1,795	10.74	7.08
120	2,274	11.04	7.45
140	2,783	11.30	7.89
160	3,311	11.54	8.19
180	3,854	11.75	8.41
200	4,407	11 94	8.69
220	4,967	12.12	9.96
240	5,531	12.28	9.22
260	6,096	12.44	9.47
280	6,662	12.58	9.71
300	7,228	12.71	9.94
320	7,792	12.84	10.17
340	8,354	12.96	10.39
360	8,914	13.07	10.60
380	9,471	13.18	10.81
400	10,024	13.28	11.02

of this steel closely resemble those of higher-purity iron. The density of samples used in these experiments, determined through immersion measurements in water on many samples, is 7.850 Mg m^{-3} with a standard deviation of 0.005 Mg m^{-3}. The theoretical density of iron is 0.3% greater [*Moses*, 1978].

Sound velocities for explosive experiments are listed in Table 1. The ratio, R, was determined using from five to ten different target thicknesses on each experiment. The Hugoniot state was characterized through measurement of shock velocities in an additional five iron samples. The standard flash gap technique [*McQueen et al.*, 1970] was used to measure U_s. Uncertainties in the shock velocity represent the standard error of the average. Particle velocities follow from a new linear $U_s - U_p$ relation for iron (J. N. Fritz and J. M. Brown, work in preparation, 1986):

$$U_s = 3.955(0.028) + 1.580(0.011)U_p \quad (8)$$

where U_s and U_p are in kilometers per second and quantities in parentheses represent 1 standard deviation uncertainties. The coefficients were determined in a new analysis of earlier data [*McQueen et al.*, 1970] for particle velocities between 1.3 km s^{-1} and 3.4 km s^{-1}. The reanalysis corrects several problems found in the old data set. With the current measurements of rarefaction sound velocities, it is now possible to recognize that some older data were incorrect due to side and back rarefaction problems. Furthermore, using theoretical calculations, small corrections have been made for explosively driven "hot" drivers. Data given by *Al'tshuler et al.* [1981] are concordant with this new fit to a particle velocity of 4.5 km s^{-1} (shock pressure of nearly 400 GPa). The old quadratic $U_s - U_p$ relation for iron [*McQueen et al.*, 1970] was constrained by data only to a pressure of 260 GPa. As previously noted [*Brown and McQueen*, 1982], the quadratic formulation cannot be successfully used in the higher-pressure regime. However, for U_p less than 1.3 km s^{-1} the quadratic formula better represents data just above the α iron to ε iron transition. Results for the current data analysis and calculations of sound velocities differ slightly from our earlier papers [*Brown and McQueen*, 1980, 1982] because equation (8) is now used.

Rankine-Hugoniot relations were used to define the shock pressure and density. Sound velocities follow from equation (3), and where appropriate, values of $\partial E/\partial P_v$ for liquid points were calculated using equation (7). Uncertainties from equation (8), and in determination of R and U_s, are fully propagated for values listed in the table.

The Hugoniot results of two-stage light-gas gun experiments are listed in Table 2. The significant difference using the gun is that projectile velocities, U_{proj}, rather than shock velocities, are measured. The uncertainty in U_{proj} is nominally 0.1% [*Brown et al.*, 1984]. For symmetric impact experiments, the particle velocity is half the projectile velocity. An additional impedance matching calculation [*McQueen et al.*, 1970] is required for experiments using tantalum impactors. The linear $U_s - U_p$ relation for tantalum is given by *Mitchell and Nellis* [1981]. Tantalum sound velocities of *Brown and Shaner* [1984] are used. The ratio R in Table 3 is the equivalent value for a symmetric impact, R_T. By equation (5), typical uncertainties in R_D cause smaller uncertainties in R_T.

Sound velocities as a function of pressure are shown in Figure 3. Data extend from just beyond the α–ε transition regime at 40 GPa [*Barker and Hollenbach*, 1974] to 400 GPa. The smooth variation in velocity from 40 GPa to the discontinuity at 200 GPa suggests that ε iron remains the stable phase in this range on the Hugoniot. A second discontinuity occurs near 240 GPa. Experiment 8C3646 is the highest-pressure point prior to a marked decrease in velocity. Above 260 GPa, data are matched by a calculated bulk sound velocity curve (equation (7)) under the assumption that $\partial E/\partial P_v$ is constant and equal to 0.051 m^3 Mg^{-1}. This is equivalent to $\rho\gamma = 19.6$ Mg m^{-3}. We therefore infer that melting occurs on the Hugoniot at a pressure of 243 ± 2 GPa. Similar Hugoniot melt-

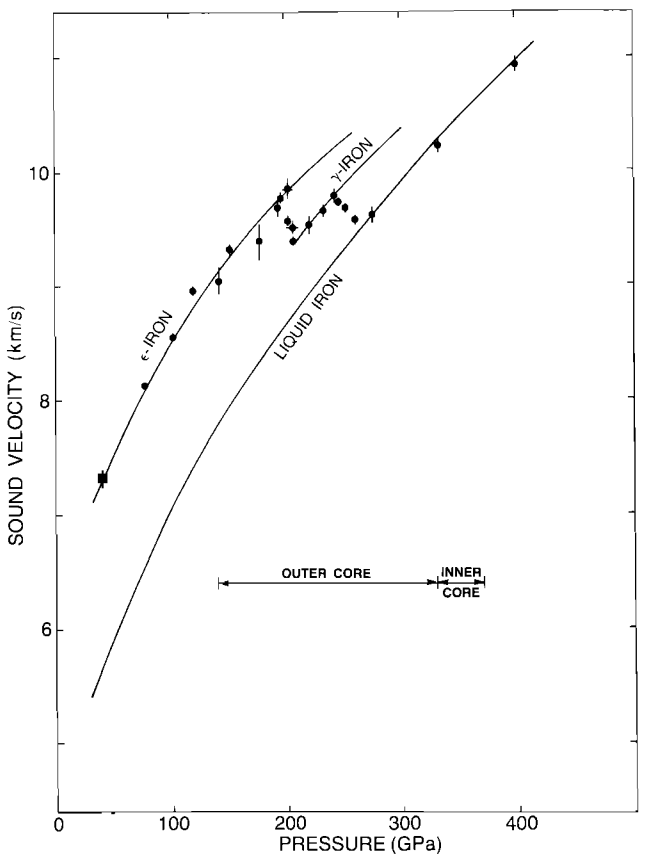

Fig. 3. Rarefaction velocities for iron on the Hugoniot as a function of pressure. Circles are present data. The square is from *Barker and Hollenbach* [1974].

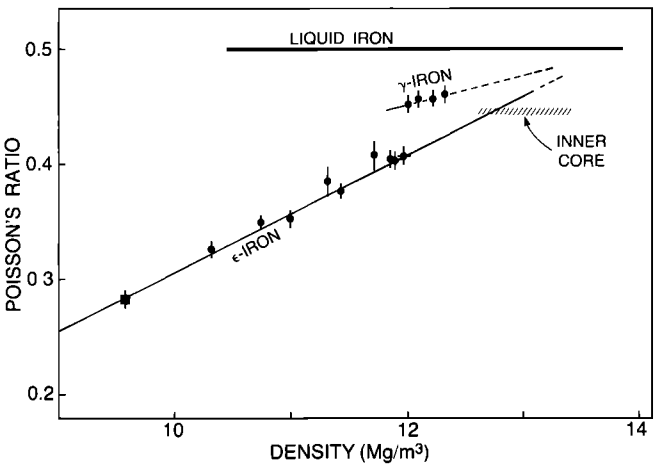

Fig. 4. Poisson's ratio as a function of density for iron on the Hugoniot and for the inner core. Circles are present data. The square is from *Barker and Hollenbach* [1974]. Data in phase transition regimes have been excluded.

ing point velocity discontinuities have been observed in tantalum and aluminum [*Shaner et al.*, 1984].

Data between 200 GPa and 243 GPa parallel trends at higher and lower pressure. If these points were interpreted to represent liquid iron behavior, a not unreasonable value of 0.08 m^3 Mg^{-1} is required for $\partial E/\partial P_v$. However, it is then difficult to explain a second (liquid-liquid) transition at 243 GPa. No such feature has been observed in other metals. Furthermore, on theoretical grounds, no electronic transition is expected in this compression range for iron [*Bukowinski and Knopoff*, 1976]. In addition, it is likely that any transition in the liquid phase would not appear as a sharp discontinuity (see, for example, *Brown et al.* [1985]). We therefore conclude that the 200-Gpa discontinuity must be a solid-solid transition. The most likely candidate based on the low-pressure phase diagram for iron is the ε–γ transition.

Poisson's ratio values were determined from the differences between the measured longitudinal velocities and calculated bulk sound velocities with $\partial E/\partial P_v = 0.051$ m^3 Mg^{-1} (Table 3). Current results are plotted in Figure 4 as a function of density. The increase in σ as a function of density along the Hugoniot reflects both temperature and compression effects. Unlike other elastic moduli, Poisson's ratio can increase both with increasing pressure and with increasing temperature (see, for example, *Anderson and Demarest* [1971] or *Falzone and Stacey* [1980]). Within each phase of solid iron the trend is quite linear; coefficients of fits are

ε iron

$$\sigma = 0.0511\rho - 0.205 \quad (9)$$

γ iron

$$\sigma = 0.0243\rho + 0.160 \quad (10)$$

where densities are in units of Mg m^{-3}. A 50% increase in the $\partial E/\partial P_v$ value used to calculate the bulk sound velocity would increase σ by approximately 10%.

MELTING OF IRON

Present results tightly constrain the density, pressure, and internal energy at the inferred Hugoniot melting point. However, temperature estimates remain less secure. We [*Brown and McQueen*, 1982] previously estimated the Hugoniot melting temperature for iron to lie between 5000 K and 6000 K. Furthermore, we noted that although the Lindemann melting criterion appeared to overestimate the pressure for melting on the Hugoniot, the criterion did provide a method for extending the fusion curve to the inner core boundary pressure of 330 GPa. Since interpretation of the present data is closely linked to the extrapolation technique and to temperature calculations, we review the thermal analysis.

The Lindemann criterion is a simplistic one-phase model based on a vibrational instability for the solid at melting. As a function of pressure along the fusion curve, the root-mean-square amplitude of atomic vibrations is assumed to remain a constant fraction of the interatomic spacing. *Wolf and Jeanloz* [1984] presented empirical evidence that high-pressure melting behavior for silicate minerals cannot be predicted on the basis of Lindemann melting. However, *Ross and Rogers* [1985] noted that changes in atomic coordination are important in accessing the validity of several "melt laws." For polyatomic, non-close-packed materials where atomic coordination changes as a function of pressure, the Lindemann criterion is not particularly useful. In contrast, close-packed monoatomic materials (like iron) appear to obey "melt laws."

The principal uncertainty in determination of the phase diagram for iron lies in the calculation of Hugoniot temperatures. In the absence of phase transitions, temperatures along the Hugoniot were calculated from basic thermodynamic relations [*McQueen*, 1964]:

$$dT = -T\left(\frac{\gamma}{V}\right)dV + \frac{1}{2C_v}\left[(V_0 - V)dP + (P - P_0)dV\right] \quad (11)$$

where C_v is the specific heat at constant volume and the differentials, dP and dV, were evaluated along the Hugoniot. The first term on the right side is the temperature increase caused by isentropic compression, while the second term arises from irreversible work during shock compression. The accuracy of Hugoniot temperature estimates is limited by uncertainties in specific heat and the Grüneisen parameter.

Although γ/V for liquid iron appears to be determined to about 5% (Tables 1 and 2), a question arises as to whether these are appropriate values for solid iron. At a room pressure density for liquid iron of 7.0 Mg m^{-3} [*Anderson*, 1982], assuming $\rho\gamma$ is constant, our value for $\partial E/\partial P_v$ predicts $\gamma_0 = 2.8$. This is significantly larger than the STP value for α iron of 1.7 [*McQueen et al.*, 1970]. In contrast, *McQueen et al.* [1984] found no more than a 10% deviation between $\partial E/\partial P_v$ values at room temperature and above the Hugoniot melting point for an aluminum alloy. *Brown and Shaner* [1984] also noted uniform behavior between solid and liquid tantalum. However, *Stevenson* [1980], using a liquid state theory, predicted larger values for γ in liquid iron. Grüneisen parameters for ε iron and γ iron have not been measured; however, theoretical estimates [*Mulargia and Boschi*, 1979] place γ_0 at less than 2. We therefore assume a lower bound for γ_0 of 1.7 and let 2.5 be the upper bound. This corresponds to approximate extremal values for $\partial E/\partial P_v$ of 0.051 m^3 Mg^{-1} and 0.075 m^3 Mg^{-1}.

In addition to the high-temperature classical lattice specific heat of $3k$ per atom, where k is Boltzmann's constant, contributions for electronic states must be included in the total heat capacity for a metal at high temperature. The specific heat is modeled:

$$C_v = D(T) + \beta_e\left(\frac{\rho_0}{\rho}\right)^{\gamma^e} T \quad (12)$$

TABLE 4. Model Hugoniot Temperatures at 200 and 243 GPa

Model	dE/dP_v, m^3/Mg	β_e, $J/Mg\ K^2$	γ_e	$\Delta T(\varepsilon-\gamma)$, K	T(200 GPa), K	T(243 GPa), K
a	0.051	11	0.67	0	5300	6990
b	0.051	91	1.34	0	4410	5620
c	0.075	91	1.34	0	4100	5250
d	0.075	91	1.34	−350	4100	4900

where $D(T)$ is the Debye function ($D(T) = 3R$ for $T > \theta$, where R is the gas constant and θ is the Debye temperature), β_e is proportional to the density of electrons at the Fermi level, and γ^e, the electronic Grüneisen parameter, describes the volume dependence for the density of states.

Although β_e can be experimentally determined at low temperatures, such determinations (even for the same solid phase) are not directly applicable to high-temperature thermodynamics [*Brown and Shaner*, 1984]. An alternative method to constrain β_e and γ^e involves band structure calculation. *Boness et al.* [1986] calculated electronic structure in both ε iron and γ iron at high pressure. The effects of high temperature on the electronic specific heats were numerically evaluated. Values for β_e and γ^e for ε iron were determined to be 90.8 J Mg^{-1} K^{-2} and 1.34 (for $\rho_0 = 8.28$ Mg m^{-3} [*Brown and McQueen*, 1982]). *Bukowinski* [1977] determined values of 80 J Mg^{-1} K^{-2} for β_e and 1.5 for γ^e from a static lattice calculation for γ iron. In contrast, the free electron approximation with eight valence electrons predicts β_e equal to 11 J Mg^{-1} K^{-2} and γ^e equal to 2/3 [*Ashcroft and Mermin*, 1976]. This large difference is caused by a peak in the density of states near the Fermi level associated with d band electrons in iron. Although we have no basis to estimate the uncertainty in the theoretical determination of electronic contributions to the specific heat, it is certain that the density of states for iron at the Fermi level must be large in comparison with the free electron approximation. At high pressures and temperatures on the Hugoniot, this means that C_v must be significantly larger than the classical lattice value.

McQueen et al. [1970] discussed the effects of phase transitions on Hugoniot temperatures. Of principal importance is the slope of the transition ($\partial P/\partial T$) which is related to both the volume and entropy changes of transition. The effect of the α–ε transition on Hugoniot temperatures is negligible [*Andrews*, 1973]; however, the higher-pressure ε–γ transition may have a significant effect. If the entropy of transition (ΔS) were independent of pressure, then based on low-pressure data by *Liu* [1975], the ε–γ transition would cause a temperature decrease along the Hugoniot of approximately 700 K at the transition [*Brown and McQueen*, 1982]. Since ΔS is likely to decrease with pressure, we propose that a decrease of 350 K is more plausible. This value is not based on rigorous theory or experimental data. Instead it is merely a reasonable order of magnitude correction.

Calculated Hugoniot temperatures, ignoring phase transitions, are given in Table 3. Table 4 lists Hugoniot temperatures at a pressure of 200 GPa (ε–γ transition) and 243 GPa (melting point) calculated for the range in parameters previously discussed. Since the free electron heat capacity is clearly an unlikely value for iron, we accept the bounds provided by other estimates. An uncertainty of over 700 K results at the Hugoniot melting point.

In Figure 5, calculated Hugoniot temperatures are plotted as a function of volume. Also shown are melting estimates based on the Lindemann melting criterion:

$$\frac{d \ln T_M}{d \ln V} = -2\gamma + 2/3 \tag{13}$$

where the Grüneisen parameter in equation (13) refers to lattice contributions only and $\rho\gamma$ was assumed to be constant for our calculations. Since electronic contributions to γ are uncertain, we use our previous bounds of $\partial E/\partial P_v = 0.051$ m^3 Mg^{-1} to 0.075 m^3 Mg^{-1}. However, only the Lindemann calculation using the lower-bound estimate for γ_0 intersects the calculated Hugoniot temperature curves close to the experimentally determined melting pressure. We use the slope of that curve in an extrapolation to the density of iron at the inner core boundary pressure of 330 GPa. This short extrapolation in density provides an estimated melting temperature of 5800 ± 500 K, at 330 GPa. This agrees with *Anderson* [1982] and is 400 K less than our previous extrapolation. Tighter constraints will require direct measurement of Hugoniot temperatures.

ELASTICITY OF IRON AND THE CORE

A long-standing complication in development of compositional constraints for the earth's core has been associated with the differing nature of laboratory and observational data. Velocity profiles through the core are better constrained than are densities (see, for example, *Masters* [1979]). In contrast, densities as a function of pressure have been the only laboratory data available for iron above 100 GPa. Differentiation of pressure-density data to obtain estimates of isentropic bulk sound velocities is subject to substantial uncertainties. Furthermore, static data have been restricted to room temperature conditions [*Jephcoat et al.*, 1986]. Thus the current data provide the first possibility for a direct comparison between seismic velocity models and laboratory data under core conditions of pressure and temperature. A geotherm (given below)

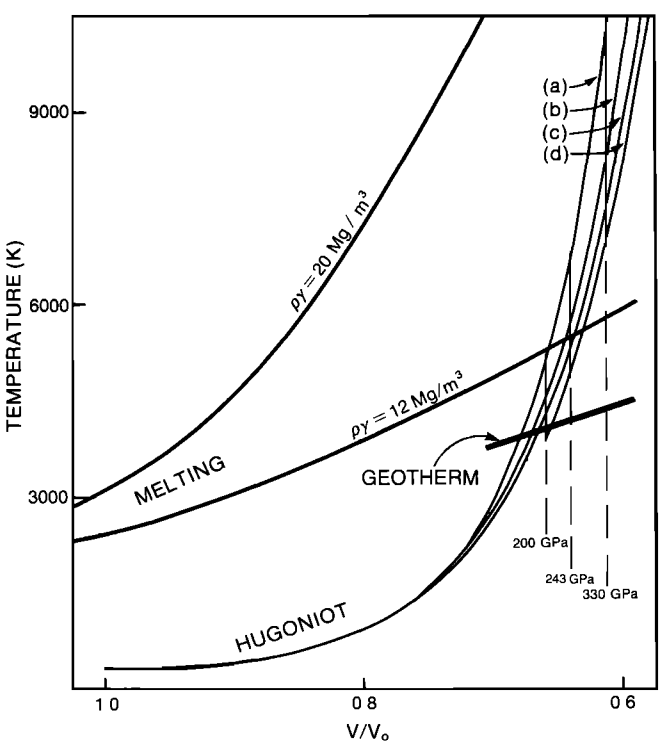

Fig. 5. Hugoniot temperatures and melting estimates based on the Lindemann criterion. Curves labeled a, b, c, and d correspond to parameters listed in Table 4

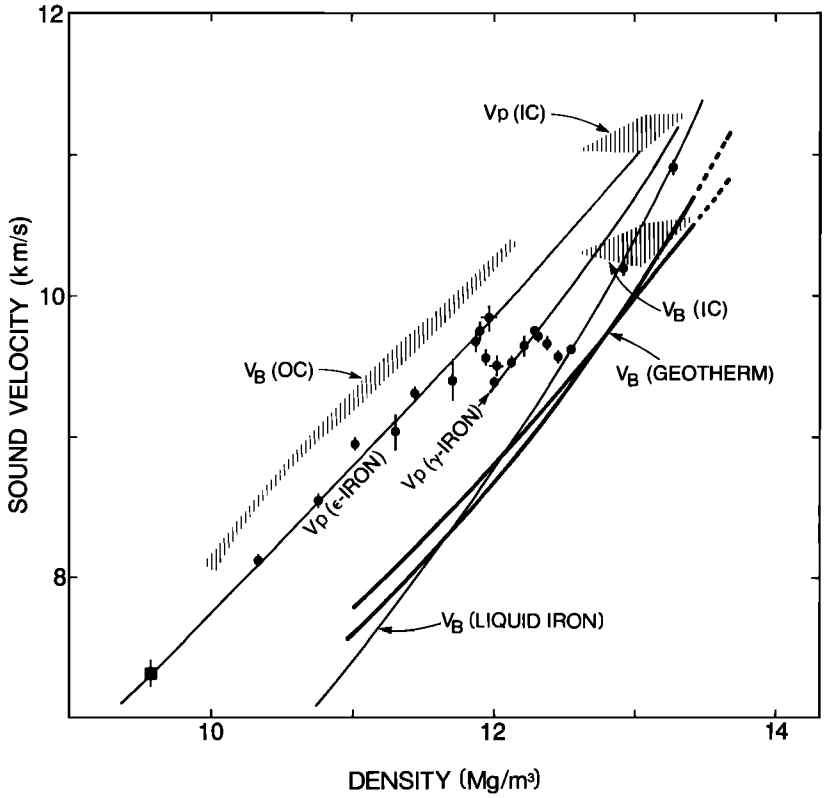

Fig. 6. Elastic wave velocities as a function of density and earth core properties from several earth models. OC is outer core; IC is inner core. The curves labeled GEOTHERM are bulk sound velocities for iron corrected from Hugoniot to core conditions. The dashed segments represent inner core conditions.

is plotted in Figure 5 to illustrate that the iron Hugoniot crosses the geotherm under outer core pressure conditions. Such behavior is preserved under large perturbations of assumptions for geotherms or the Hugoniot parameters.

In accordance with velocity-density systematics [*Shankland*, 1977], the current data for iron are shown in Figure 6 as a function of density. Such a representation incorporates much (but not all) of the variation of velocity as a function of temperature and pressure through its volume dependence. Also represented are envelopes enclosing earth model profiles. These include 1066A and 1066B [*Gilbert and Dziewonski*, 1975] and PREM [*Dziewonski and Anderson*, 1981]. Profiles for the liquid outer core represent the bulk sound velocity. Both compressional and bulk velocities are plotted for the solid inner core. The relative uncertainty in inner core density is illustrated by broad crosshatched regions.

Curves representing both bulk and compressional velocities for iron along the Hugoniot are also shown in Figure 6. Bulk sound velocities are from Table 3. In the absence of a theory to provide a basis for calculation of the pressure and temperature dependences of Poisson's ratio for ε iron and γ iron, the linear trends established in the preceding section are used for extrapolation. This approach preserves a reasonable behavior for σ. Near melting, σ is large but is less than the liquid value of 0.5. However, since Poisson's ratio is quite structure sensitive [*Anderson and Demarest*, 1971], present extrapolations are subject to uncertainty.

Thermal corrections to bulk sound velocities along a core geotherm are calculated through Mie-Grüneisen theory [*McQueen et al.*, 1970] in the following manner. Pressure, temperature, and bulk sound velocities are calculated along the Hugoniot as a function of volume. A thermal pressure offset (P_t) at a given volume is calculated from

$$P_t = P - P_H = \left(\frac{\gamma}{V}\right)\left[3R(T - T_H) + \frac{\beta_e}{2}\left(\frac{V}{V_0}\right)^{\gamma^e}(T^2 - T_H{}^2)\right] \tag{14}$$

where subscript H refers to the Hugoniot state, $3R$ is the high-temperature Dulong-Petit lattice specific heat, and P and T are the off-Hugoniot conditions. The correction to the bulk sound velocity is given by

$$C^2 = C_H{}^2 + V^2 P_t\left(\frac{\gamma}{V}\right) \tag{15}$$

where $\gamma/V = \text{const}$ was assumed in this derivation. A core geotherm with temperatures ranging from 3800 K at the core-mantle boundary to 5000 K at the earth's center was used. Motivation for this geotherm is given below. Two geotherm velocity profiles for iron are shown in Figure 6. One is based on the empirical fit to Hugoniot data (equation (8)) while the other is calculated using the metastable ε iron Hugoniot given by *Brown and McQueen* [1982]. These two examples provide an estimation of the sensitivity of results to model assumptions. At constant density, the two models differ by at most 4%, while velocities between the Hugoniot and geotherm differ by less than 10%. A similar relation between compressional velocities on the Hugoniot and on the geotherm is plausible. Thus under inner core conditions, solid iron velocities are likely to lie below the extrapolated Hugoniot trends.

Seismic velocity profiles for the outer core are approximately 10% higher than the calculated bulk sound velocities for pure iron at the same density. Such a difference is most likely associated with the presence of elements having atomic weights lower than iron. This conclusion is in agreement with the observation that light elements are also required to match

core densities (*Brown et al.* [1984], *Jeanloz* [1979], and many references therein). Although not a new observation, the principal value of the present work is that seismic velocity profiles are more directly compared with laboratory results.

Based on mean-atomic-weight systematics, the velocity profile of a chemically homogeneous outer core should be parallel to that of iron. In Figure 6, bulk velocities for iron are approximately parallel, although the range predicted for iron is greater than that observed for the core. More thorough compositional constraints will require laboratory data for iron alloys. Such studies are now in progress.

For the inner core, bulk sound velocities of iron on the Hugoniot trend through the earth model range. However, predicted velocities and densities for iron on the geotherm are slightly larger (by 10% or less) than average values for the inner core. Such deviations may reflect both poor seismic resolution and uncertain thermal corrections for the equation of state of iron. Alternatively, an inner core composition differing from pure iron cannot be excluded. However, on the basis of current data, it is unlikely that the inner core contains significant amounts (greater than a few percent) of lower-atomic-weight materials.

Such a compositional constraint for the inner core is consistent with the chemical-thermodynamic equilibrium model for its formation. Given an outer core composition on the iron-rich side of a eutectic, the inner core may represent the first (near iron end-member) crystallization from a cooling outer core liquid that is becoming increasingly enriched in the lighter components. We previously used this eutectic model to estimate the equilibrium temperature of crystallization at the inner core boundary [*Brown and McQueen*, 1982]. Incorporation of the current revision for the melting point temperature of pure iron leads to the geotherm given here.

Although earth model estimations for the inner core are divergent, compressional velocities are better matched by the extrapolated curves for ε iron. Poisson's ratios for γ iron appear too large (see also Figure 4). Corrections from Hugoniot conditions to the geotherm are likely to decrease compressional velocities and make pure γ iron even less tenable as an inner core constituent. This observation further supports the validity of the phase diagram for iron given by *Brown and McQueen* [1982]. That work predicted the existence of a triple point of γ, ε, and liquid iron near the inner core boundary pressure of 330 GPa. The stable pure iron phase under inner core conditions was thus suggested to be ε iron.

As noted by *Falzone and Stacey* [1980, and references therein], the observed value of Poisson's ratio for the inner core ($\sigma = 0.44$) has been considered somewhat anomalous. This has generated speculation concerning the state of matter in the inner core (see, for example, *Anderson* [1983]). However, the present results and previous work on other metals [*Shaner et al.*, 1984] suggest that values for Poisson's ratio of approximately 0.45 are normal for metals at high pressure and temperature. On the basis of these sound velocity measurements, seismic properties for the inner core appear typical, rather than anomalous, for solids.

CONCLUSION

Sound velocity data for iron have been obtained over a pressure regime between 77 GPa and 400 GPa. Two major discontinuities in elastic sound velocities provide a basis for the interpretation of thermal and chemical conditions in the earth's core. An upper bound for temperature at the inner core boundary is based on the melting of pure iron. The Hugoniot melting point at 243(2) GPa provides a tie point in a Lindemann criterion extrapolation to a pressure of 330 GPa. The melting temperature estimate of 5800 $\pm$ 500 K for pure iron at the inner core boundary is based on calculations using plausible bounds for specific heat and experimental constraints for the Grüneisen parameter. A core geotherm ranging from 5000 K at the earth's center to 3800 K at the core-mantle boundary is suggested.

Comparison between bulk sound velocities of iron and the outer core supports the widely accepted hypothesis that the outer core is predominately iron mixed with elements of lower atomic weight. Velocities in the inner core, however, strongly suggest a nearly pure iron composition. Furthermore, if no light elements are present in the inner core, compressional velocities for ε iron best match inner core properties. The elastic properties of the inner core appear to represent normal high-pressure, high-temperature behavior for a solid metal.

Acknowledgments. Support for this work came from the National Science Foundation (originally EAR 75-09504 and more recently from EAR 81-09591 and EAR 85-01390) and from the Department of Energy. We thank G. H. Shaw (Department of Geology and Geophysics, University of Minnesota, Minneapolis) for initial support enabling J.M.B. to undertake these studies. The following individuals have helped in undertaking experiments: D. Shampine, R. Medina, R. Holt, A. Bonner, S. Salezar, J. Chavez, F. Depaulo, C. Gomez, D. Martinez, and V. Gurule. We appreciate their efforts. Comments and discussions with the following people have also been important: J. Fritz, J. Shaner, T. Ahrens, T. Shankland, and R. Jeanloz.

REFERENCES

Ahrens, T. J., Equations of state of iron sulfide and constraints on the sulfur content of the earth, *J. Geophys. Res.*, *84*, 985–998, 1979.

Akimoto, S., and Y. Syono, The coesite-stishovite transition, *J. Geophys. Res.*, *74*, 1653–1659, 1969.

Al'tshuler, L. V., S. B. Kormer, M. I. Brazhnik, L. A. Vladimirov, M. P. Speranskaya, and A. I. Funtikov, The isentropic compressibility of aluminum, copper, lead, and iron at high pressures, *Sov. Phys. JETP*, Engl. Transl., *11*, 766–775, 1960.

Al'tshuler, L. V., M. I. Brazhnik, and G. S. Telegin, Strength and elasticity of iron and copper at high shock-wave compression pressures, *J. Appl. Mech Tech. Phys.*, Engl. Transl., *12*, 921–926, 1971.

Al'tshuler, L. V., A. A. Bakanova, I. P. Dudoladov, E. A. Dynin, R. F. Trunin, and B. S. Chekin, Shock adiabatic curves of metals: New data, statistical analysis, and general laws, *J. Appl. Mech. Tech. Phys.*, Engl. Transl., *22*, 145–169, 1981.

Anderson, D. L., A new look at the inner core of the earth, *Nature*, *302*, 660, 1983.

Anderson, O. L., The earth's core and the phase diagram of iron, *Philos. Trans. R. Soc. London, Ser. A*, *306*, 21–35, 1982.

Anderson, O. L., and H. H. Demarest, Jr., Elastic constants of the central force model for cubic structures: Polycrystalline aggregates and instabilities, *J. Geophys. Res.*, *76*, 1349–1369, 1971.

Andrews, D. J., Equation of state of the alpha and epsilon phases of iron, *J. Phys. Chem. Solids*, *34*, 825–840, 1973.

Asay, J. R., Shock loading and unloading in bismuth, *J. Appl. Phys.*, *48*, 2832–2844, 1977.

Asay, J. R., and D. B. Hayes, Shock-compression and release behavior near melt states in aluminum, *J. Appl. Phys.*, *46*, 4789–4799, 1975.

Ashcroft, N. W., and N. D. Mermin, *Solid State Physics*, 826 pp., Holt, Rinehart and Winston, New York, 1976.

Barker, L. M., and R. E. Hollenbach, Shock wave study of the alpha-epsilon phase transition in iron, *J. Appl. Phys.*, *45*, 4872–4887, 1974.

Beck, G., Operation of a 1P28 photomultiplier with subnanosecond response time, *Rev. Sci. Instrum.*, *47*, 537–541, 1976.

Boness, D. A., J. M Brown, and A. K. McMahan, Electronic specific heat of iron under earth core conditions, *Phys. Earth Planet. Inter.*, in press, 1986.

Brown, J. M., and R. G. McQueen, Melting of iron under core conditions, *Geophys. Res. Lett.*, *7*, 533–536, 1980.

Brown, J. M., and R. G. McQueen, The equation of state for iron and the earth's core, in *High-Pressure Research in Geophysics*, vol. 12, edited by S. Akimoto and M. H. Manghnani, pp. 611–623, Center for Academic Publications, Tokyo, 1982.

Brown, J. M., and J. W. Shaner, Rarefaction velocities in shocked tantalum and the high pressure melting point, in *Shock Waves in Condensed Matter*, edited by J. R. Asay, R. A. Graham, and G. K. Straub, pp. 91–94, Elsevier, New York, 1984.

Brown, J. M., T. J. Ahrens, and D. L. Shampine, Hugoniot data for pyrrhotite and the earth's core, *J. Geophys. Res.*, *89*, 6041–6048, 1984.

Brown, J. M., C. A. Swenson, and J. W. Shaner, Shock determination of the Grüneisen parameter for lanthanum and the *6s–5d* transition, *Phys. Rev. B*, *32*, 4507–4512, 1985.

Bukowinski, M. S. T., A theoretical equation of state for the inner core, *Phys. Earth Planet. Inter.*, *14*, 333–344, 1977.

Bukowinski, M. S. T., and L. Knopoff, Electronic structure of iron and models of the earth's core, *Geophys. Res. Lett.*, *3*, 45–48, 1976.

Bundy, F. P., The *P*, *T* phase and reaction diagram for elemental carbon, 1979, *J. Geophys. Res.*, *85*, 6930–6936, 1980.

Davison, L., and R. A. Graham, Shock compression of solids, *Phys. Rep.*, *55*, 255–379, 1979.

Dziewonski, A. M., and D. L. Anderson, Preliminary reference earth model, *Phys. Earth Planet. Inter.*, *25*, 297–356, 1981.

Falzone, A. J., and F. D. Stacey, Second-order elasticity theory: Explanation for the high Poisson's ratio of the inner core, *Phys. Earth Planet. Inter.*, *21*, 371–377, 1980.

Furnish, M. D., and W. A. Bassett, Investigation of the mechanism of the olivine spinel transition in fayalite by synchrotron radiation, *J. Geophys. Res.*, *88*, 10,333–10,341, 1983.

Gilbert, F., and A. M. Dziewonski, An application of normal mode theory to the retrieval of structural parameters and source mechanisms from seismic spectra, *Philos. Trans. R. Soc. London, Ser. A*, *278*, 187–269, 1975.

Grady, D. E., and J. R. Asay, Calculation of thermal trapping in shock deformation of aluminum, *J. Appl. Phys.*, *53*, 7350–7354, 1982.

Holian, B. L., and G. K. Straub, Molecular dynamics of shock waves in three-dimensional solids: Transition from nonsteady to steady waves in perfect crystals and implications for the Rankine-Hugoniot conditions, *Phys. Rev. Lett.*, *43*, 1598–1600, 1979.

Jamieson, J. C., and A. W. Lawson, X-ray diffraction studies to 100 kbar, *J. Appl. Phys.*, *33*, 776–780, 1962.

Jamieson, J. C., H. H. Demarest, Jr., and D. Schiferl, A reevaluation of the Grüneisen parameter for the earth's core, *J. Geophys. Res.*, *83*, 5929–5935, 1978.

Jeanloz, R., Properties of iron at high pressure and the state of the core, *J. Geophys. Res.*, *84*, 6059–6069, 1979.

Jephcoat, A. P., H. Mao, and P. M. Bell, The static compression of iron to 78 GPa with rare gas solids as a pressure-transmitting media, *J. Geophys. Res.*, *91*, 1986.

Johnson, P. C., B. A. Stein, and R. S. Davis, Temperature dependence of shock-induced phase transformation in iron, *J. Appl. Phys.*, *33*, 557–561, 1962.

Johnson, Q., and A. C. Mitchell, First x-ray diffraction evidence for a phase transition during shock compression, *Phys. Rev. Lett.*, *29*, 1369–1371, 1972.

Kondo, K., and T. J. Ahrens, Heterogeneous shock-induced thermal radiation in minerals, *Phys. Chem. Miner.*, *9*, 173–181, 1983.

Liu, L. G., On the (γ, ε, 1) triple point of iron and the earth's core, *Geophys. J. R. Astron. Soc.*, *43*, 697–705, 1975.

Mao, H. K., W. A. Bassett, and T. Takahashi, Effect of pressure on crystal structure and lattice parameters of iron up to 300 kbar, *J. Appl. Phys.*, *38*, 272–276, 1967.

Marsh, S. P., *Shock Hugoniot Data*, p. 658, University of California Press, Los Angeles, 1980.

Masters, G., Observational constraints on the chemical and thermal structure of the earth's deep interior, *Geophys. J. R. Astron. Soc.*, *57*, 507–534, 1979.

McQueen, R. G., Laboratory techniques for very high pressures and the behavior of metals under dynamic loading, in *Conference on Metallurgy at High Pressure*, vol. 22, edited by K. A. Gschneider, M. T. Hepworth, and N. A. D. Parlee, pp. 44–132, Gordon and Breach, New York, 1964.

McQueen, R. G., S. P. Marsh, J. W. Taylor, J. N. Fritz, and W. J. Carter, The equation of state of solids from shock wave studies, in *High-Velocity Impact Phenomena*, edited by R. Kinslow, pp. 244–419, Academic, Orlando, Fla., 1970.

McQueen, R. G., J. W. Hopson, and J. N. Fritz, Optical technique for determining rarefaction wave velocities at very high pressures, *Rev. Sci. Instrum.*, *53*, 245–250, 1982.

McQueen, R. G., J. N. Fritz, and C. E. Morris, The velocity of sound behind strong shock waves in 2024 Al, in *Shock Waves in Condensed Matter*, edited by J. R. Asay, R. A. Graham, and G. K. Straub, pp. 95–98, Elsevier, New York, 1984.

Mitchell, A. C., and W. J. Nellis, Shock compression of aluminum, copper and tantalum, *J. Appl. Phys.*, *52*, 3363–3374, 1981.

Morris, C. E., and J. N. Fritz, Relation of the "solid Hugoniot" to the "fluid Hugoniot" for aluminum and copper, *J. Appl. Phys.*, *51*, 1244–1246, 1980.

Moses, A. J., *The Practicing Scientist's Handbook*, p. 1291 Van Nostrand-Reinhold, New York, 1978.

Mulargia, F., and E. Boschi, Equations of state of close-packed phases of iron and their implications for the earth's core, *Phys. Earth Planet. Inter.*, *18*, 13–19, 1979.

Ramakrishnan, J., R. Boehler, G. H. Higgins, and G. C. Kennedy, Behavior of Grüneisen's parameter of some metals at high pressures, *J. Geophys. Res.*, *83*, 3535–3558, 1978.

Ross, M., and F. J. Rogers, Structure of dense shock-melted alkali halides: Evidence for a continuous pressure induced structural transition in the melt, *Phys. Rev. B*, *31*, 1463–1468, 1985.

Shaner, J. W., J. M. Brown, and R. G. McQueen, Melting of metals above 100 GPa, in *High Pressure in Science and Technology*, vol. 22, edited by C. Homan, R. K. MacCrone, and E. Whalley, pp. 137–141, North-Holland, New York, 1984.

Shankland, T. J., Elastic properties, chemical composition, and crystal structure of minerals, *Geophys. Surv.*, *3*, 69–100, 1977.

Stevenson, D. J., Application of liquid state physics to the earth's core, *Phys. Earth Planet. Inter.*, *22*, 42–52, 1980.

Swenson, C. A., J. M. Brown, and J. W. Shaner, Hugoniot sound velocity measurements on CsI and the insulator-to-metal transition, *Phys. Rev. B*, in press, 1986.

Wackerle, J., Shock-wave compression of quartz, *J. Appl. Phys.*, *33*, 922–937, 1962.

Wolf, G. H., and R. Jeanloz, Lindemann melting law: Anharmonic correction and test of its validity for minerals, *J. Geophys. Res.*, *89*, 7821–7835, 1984.

J. M. Brown, Geophysics Program, University of Washington, Seattle, WA 98195.

R. G. McQueen, Shock-Wave Physics Group, Los Alamos National Laboratory, Los Alamos, NM 87545.

(Received October 18, 1985;
revised February 12, 1986;
accepted February 18, 1986.)